Dynamics, Energetics, and Structure in Protein Folding[†]

Athi N. Naganathan, Urmi Doshi, Adam Fung, Mourad Sadqi, and Victor Muñoz*

Department of Chemistry and Biochemistry and Center for Biomolecular Structure and Organization, University of Maryland, College Park, Maryland 20742

Received April 1, 2006; Revised Manuscript Received June 5, 2006

ABSTRACT: For many decades, protein folding experimentalists have worked with no information about the time scales of relevant protein folding motions and without methods for estimating the height of folding barriers. Protein folding experiments have been interpreted using chemical models in which the folding process is characterized as a series of equilibria between two or more distinct states that interconvert with activated kinetics. Accordingly, the information to be extracted from experiments was circumscribed to apparent equilibrium constants and relative folding rates. Recent developments are changing this situation dramatically. The combination of fast-folding experiments with the development of analytical methods more closely connected to physical theory reveals that folding barriers in native conditions range from minimally high (∼14*RT* for the very slow folder AcP) to nonexistent. While slow-folding (i.e., ≥1 ms) single-domain proteins are expected to fold in a two-state fashion, microsecond-folding proteins should exhibit complex behavior arising from crossing marginal or negligible folding barriers. This realization opens a realm of exciting opportunities for experimentalists. The free energy surface of a protein with a marginal (or no) barrier can be mapped using equilibrium experiments, which could resolve energetic factors from structural factors in folding. Kinetic experiments on these proteins provide the unique opportunity to measure folding dynamics directly. Furthermore, the complex distributions of time-dependent folding behaviors expected for these proteins might be accessible to single-molecule measurements. Here, we discuss some of these recent developments in protein folding, emphasizing aspects that can serve as a guide for experimentalists interested in exploiting this new avenue of research.

In folding to their biologically active 3D[1] structures, proteins must coordinate the vast number of degrees of freedom of their polypeptide chains by forming complex networks of noncovalent interactions. Therefore, understanding protein folding involves determining the relations between the energetics of weak interactions and protein conformation and the collective chain dynamics that govern the search in conformational space. In modern rate theory, these issues are resolved by mapping the potential energy of the molecule as a function of the relevant coordinates. The dynamics are then represented as diffusion on such an energy surface (*1*, *2*). For folding reactions, however, even the solvent-averaged free energy surface is hyperdimensional due to the large number of relevant coordinates (i.e., thousands of atomic coordinates for a small protein) (*3*). Folding hypersurfaces should also be topographically complex due to frustration among the myriad of possible interactions (*3*, *4*). Moreover, molecular simulations (*5*−*8*) and NMR dynamics experiments (*9*) indicate that protein conformational motions span a wide range of time scales (i.e., from picoseconds to milliseconds). The implication is that measuring folding surfaces experimentally would require detection of single-protein molecules with full atomic detail and subnanosecond resolution during long periods of time. Obviously, such measurements are well beyond our current experimental capabilities.

To complicate matters further, protein folding reactions appear deceivingly simple in traditional thermodynamic and kinetic experiments (*10*). Accordingly, it has been customary to interpret folding experiments as elementary chemical reactions. Protein thermodynamics are then discussed in terms of chemical equilibria between a series of discrete macrostates (*11*), which interconvert with activated kinetics over arbitrarily high free energy barriers (*12*). The simplicity of the chemical approach has made it extremely popular in the folding field (*10*). However, interpreting protein folding as a simple chemical reaction carries a significant amount of baggage. The dimensionality and shape of the folding free energy surface are assumed implicitly and, thus, cannot be investigated experimentally. Furthermore, the information that can be obtained from experiments is limited to equilibrium and rate constants in which energetic, dynamic, and structural factors are all intertwined. In other words, by describing folding in chemical terms, we are giving up the opportunity to measure experimentally the very same fundamental properties that determine folding mechanisms and are most relevant in comparisons with theory.

In this light, the divide between classical folding experimentalists and theorists should be hardly surprising (*13*). This divide has been bridged in part by the spectacular develop-

[†] The research described here has been supported by NIH Grant GM-066800 and NSF Grant MCB-0317294.

* To whom correspondence should be addressed. Phone: (301) 405-3165. Fax: (301) 405-0386. E-mail: vmunoz@umd.edu.

[1] Abbreviations: 3D, three-dimensional; NMR, nuclear magnetic resonance; CD, circular dichroism; DSC, differential scanning calorimetry; AcP, muscle acyl phosphatase.

10.1021/bi060643c CCC: $33.50
Published on Web 06/22/2006

ment of computer simulations (*6*−*8*, *14*−*16*) together with a shift in experimental focus toward fast-folding proteins (*17*−*22*). The microsecond folding time scales of these proteins make it possible to connect with modern simulations, which are finally reaching comparable time scales. Furthermore, work of fast-folding proteins has produced significant evidence indicating that folding barriers are small, sometimes even absent altogether. Such observations have confirmed critical theoretical predictions. Moreover, the existence of small folding barriers opens a new realm of opportunities for the experimental analysis of protein folding. With marginal folding barriers, it becomes possible to extricate dynamic factors from energetic factors in kinetic experiments and resolve energetic contributions and structural ensembles in equilibrium folding experiments. Here we discuss recent developments in this area, which are paving the way for a shift from the traditional biochemical paradigm to a physical paradigm in experimental protein folding.

Free Energy Projections and Reaction Coordinates

Hyperdimensional free energy surfaces can be greatly simplified by projecting them onto one or a few order parameters. The resulting low-dimensional free energy projections then provide a bridge that connects theory, simulation, and experiment. The application of this approach to protein folding, which was pioneered by Wolynes and collaborators (*3*, *4*, *23*, *24*) and has become a very popular tool for the analysis of computer simulations (*16*, *25*−*27*), explains the two-state-like folding exhibited by many proteins. It also predicts the existence of barrierless folding and other complex kinetic behaviors (*3*). In principle, the approach should be extensible to the direct interpretation of folding experiments. What is not so clear a priori is whether a surface of very low dimensionality, or even of one dimension, can reproduce folding reactions effectively or what order parameters might behave as reaction coordinates.

Here, it is interesting to note that the chemical two-state model is a simplified representation of a one-dimensional free energy surface with a high barrier separating two minima. Therefore, the apparent success of two-state analyses already suggests that even one-dimensional projections may suffice in describing coarse folding properties. The first direct evidence supporting the validity of one-dimensional folding surfaces has come from the analysis of simulations in the cubic lattice (*28*). Further support comes from the reasonable success in calculating relative folding rates from protein structures using one-dimensional free energy surfaces (*29*). More recently, the performance of one-dimensional free energy projections has been tested empirically for the case of α-helix formation (*30*). The analysis took advantage of a detailed kinetic theory for α-helix formation that explains quantitatively the complex observations of Gai and collaborators in laser-induced temperature-jump experiments with isotopically labeled helical peptides (*31*−*33*). This allows for direct comparison among experiment, detailed theory, and the free energy projection approach. The kinetic theory is an extension of nucleation−elongation helix−coil equilibrium models in which helix segments nucleate at any point in the sequence and grow longer from their ends (*34*). The nucleation−elongation mechanism produces complex kinetics with hundreds of thousands of coupled differential equations and a myriad of possible pathways. Remarkably,

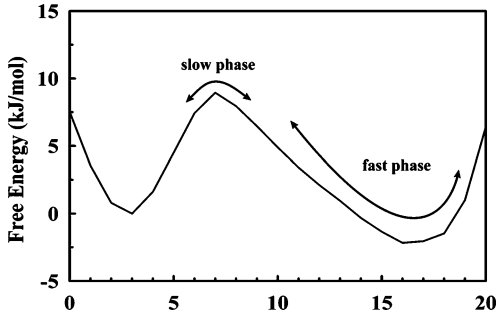

FIGURE 1: One-dimensional free energy surface for α-helix formation obtained by projecting the free energy of all of the species from the detailed kinetic model as a function of the number of helical peptide bonds. The arrows represent the main flux involved in each of the two observable kinetic phases.

the projection of the multidimensional free energy surface onto one order parameter (i.e., the number of helical peptide bonds) reproduced the observed kinetics with surprising accuracy. The agreement went to the level of matching the relative amplitudes for the characteristic slow and fast phases of helix−coil kinetics. Furthermore, the diffusion coefficient from the surface analysis was essentially identical to the elementary peptide bond rotation rate [$\sim$1/(2 ns)] in the kinetic theory, indicating that the number of helical peptide bonds is a good reaction coordinate for α-helix formation (*30*). These results validate a one-dimensional free energy projection on a folding-related problem for which the mechanism is reasonably well understood. The free energy surface analysis of α-helix formation also exemplifies some of the features expected for protein folding reactions with marginal barriers. Because the barrier is very small ($\sim$2*RT*), the relaxation process is expected to exhibit two phases (Figure 1). The fast phase involves the relaxation in the broad helical minimum, which is diffusive. The somewhat slower phase consists of the re-equilibration between both sides of the barrier and, thus, has diffusive and activated terms. This same kinetic behavior has recently been observed in fast-folding mutants of λ repressor (*35*). From the emergence of an additional, faster, kinetic phase in the mutants, Gruebele and collaborators concluded that these proteins folded by crossing a marginal folding barrier (*35*). The same mutants lost the slow kinetic phase when highly stabilized by cosolvents, suggestive of downhill folding under those conditions (*36*).

Protein folding is obviously more complex than helix formation, involving large changes in overall shape and compaction. The greater complexity in folding is likely to result in diffusion coefficients that change with the value of the order parameter. These changes would reflect the different dynamic modes controlling overall protein motions and the increasing surface roughness as the protein becomes more folded (i.e., more compact) (*3*). Effective diffusion coefficients for folding on a one-dimensional energy surface are therefore expected to be complex functions of the order parameter, including both dynamic and energetic terms (*28*).

Motions in Protein Folding

Although most experimentalists have focused on the energetic and structural aspects of folding, the dynamic modes that govern polypeptide chain motions are critical components of folding mechanisms. The time scales for the

relevant folding motions provide upper limits for the effective diffusion coefficient for folding, which are required for estimation of barrier heights from folding rates using the simple rate expression

$$k = D_{\text{eff}} \exp(-\Delta G^{\ddagger}/RT) \quad (1)$$

This is far from being a trivial point. Without an independent estimate of either the diffusion coefficient or the barrier height, protein folding rates can be analyzed in only relative terms [e.g., differences between the wild type and mutant (*37*)]. Furthermore, an Arrhenius analysis of the temperature dependence of the folding rate can be seriously misleading because (i) the barrier and the diffusion coefficient have both temperature-dependent and temperature-independent contributions, (ii) the hydrophobic effect results in large enthalpy−entropy compensations (*38*), and (iii) glassy dynamics may arise at low temperatures (*3*).

Fortunately, our understanding of protein folding motions has improved significantly in recent years. The detailed kinetic analysis of α-helix and β-hairpin formation indicates that local motions (i.e., peptide bond rotations) with time scales of ∼1−10 ns control secondary structure formation (*39*, *40*). These local motions presumably dominate the dynamics of expanded random coil polypeptides, in which there are not significant structural correlations. It is noteworthy that this peptide bond rotation rate already has an energetic term (i.e., activation energy) equivalent to ∼20−25 kJ/mol (*40*), which arises from chain steric hindrance and changes in water viscosity. The rate of end-to-end contact formation in unstructured chains has been measured for several sequences and conditions, and with a variety of methods (*41*−*45*). The time scales cluster in the few tens of nanoseconds, providing a good estimate for the concerted motions leading to loop formation in protein folding (*22*). The overall motions of a denatured but collapsed polypeptide are even slower. A time scale of ∼100 ns has recently been measured for the random collapse of a 40-residue protein (*46*). This collapse time scales to ∼500 ns for a protein domain of 100 residues. The slower time scales of these motions reflect coupling of many local rotations into a single global mode, which slows as the protein becomes more compact (*46*). The chain dynamics of collapsed denatured proteins are probably similar to the dynamics in early stages of folding, in which the protein is already compact but has few specific tertiary interactions.

As the protein becomes more folded and tertiary interactions more consolidated, chain motions should slow further because the changes in conformation are likely to involve breaking of preformed interactions. At this point, the energetic terms in the diffusion coefficient (i.e., the roughness of the landscape) might be quite large (*4*). A dramatic demonstration of this effect is seen in the rate of collapse of unfolded cytochrome *c*, in which the strong nonspecific interactions with the heme slow the collapse rate to hundreds of microseconds (*47*−*50*). The experiments with the fast-folding mutants of λ repressor (see the previous section) suggest that the effective diffusion coefficient for folding of this protein is ∼1/(2 μs) at 340 K (*35*). A diffusion coefficient of ∼1/(8 μs) has also recently been estimated for cytochrome *c* at 298 K (*51*). It is thus clear that the average folding speed limit, and therefore the dynamic term to use in eq 1, is on the microsecond time scale for natural proteins near 298 K. These values are surprisingly close to the original estimate of Eaton and co-workers (*52*), which was based on the rate of contact formation in chemically unfolded cytochrome *c*, and ∼7 orders of magnitude slower than the gas-phase frequency factor ($k_B T/h$).

It is important to keep in mind the fact that the diffusion coefficient should depend on experimental conditions (e.g., temperature and solvent viscosity), protein structure, protein sequence and size, and the position of the top of the barrier along the reaction coordinate. For example, hyperfast-folding mutants or de novo designed proteins, in which secondary structure propensities are typically maximized, are likely to tip the top of the folding barrier toward the unfolded state, thereby changing the relevant dynamic regime to that of a less compact ensemble (i.e., faster dynamics). Some of these engineered proteins might fold in less than 1 μs (*53*). By the same token, the use of a simple rate equation (eq 1) yields reasonable results when the barrier is sufficiently high (i.e., several *RT*). Under those conditions, the diffusion coefficient reflects the dynamics at the top of the barrier. However, this treatment breaks down as the barrier heights decrease. For proteins with marginal barriers, the rate becomes increasingly diffusive and separates into two observable phases (see Figure 1). Although it may seem counterintuitive, for downhill-folding proteins the observed folding rate might actually decrease again, the reason being that under strongly native conditions the diffusive downhill relaxation will be dominated by slow dynamics near the native well. Equation 1 should be used only for slow-folding proteins (millisecond or longer folding times) and while keeping in mind the fact that the use of an average diffusion coefficient inevitably introduces error into the estimation of the folding barriers.

Free Energy Barriers to Folding

The application of eq 1 parametrized with the empirical estimates of the diffusion coefficient [i.e., from 1/(20 ns) to 1/(5 μs)] to several proteins previously catalogued as two-state (CI2, protein L, FKBP12, Im9, CspB, and GCN4) indicated that their barrier heights under native conditions are typically $<10RT$ (*54*). These barriers are sufficiently high to result in apparent two-state kinetics, in agreement with their classification as two-state-like. However, for some of them, the barrier is sufficiently low to suggest that strongly destabilizing mutations might result in departures from two-state behavior. The rate analysis for these six two-state proteins offered another valuable piece of information. Namely, it confirmed experimentally that folding barriers arise from the nonsynchronous decrease in conformational entropy and gain in stabilization free energy (Figure 2). The origin of the folding barriers became apparent when the activation free energy as a function of temperature derived from eq 1 was analyzed thermodynamically with the approach developed by Freire and co-workers for equilibrium thermal unfolding (*55*). This analysis produced very similar results for the six proteins: at the top of the folding barrier, these proteins had lost ∼36% of their conformational entropy and gained only ∼27% in stabilization free energy. This very small relative difference can still result in barriers of several *RT* because both compensating terms are large (i.e., for a protein of 65 residues with a cost in conformational entropy of 17.5 J mol^{-1} K^{-1} per residue the 36/27 ratio produces a

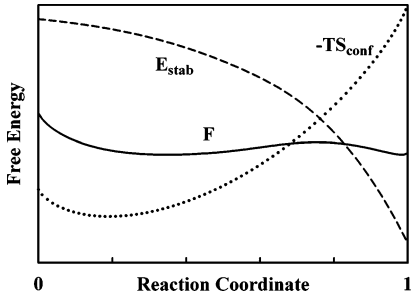

FIGURE 2: Representation of a one-dimensional folding free energy surface: stabilization free energy (− − −), conformational entropy contribution (···), and global free energy (—). The height of the free energy barrier is ~20 kJ/mol.

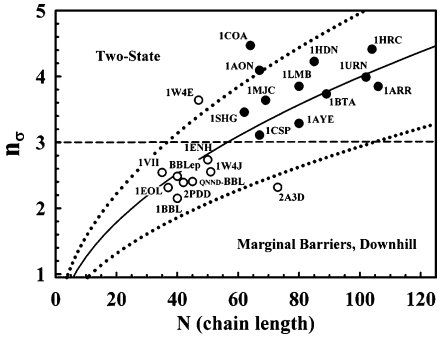

FIGURE 3: Plot of the n_σ parameter vs the number of amino acids (N) for several proteins with T_m values near 333 K. Proteins are named with their Protein Data Bank code. The solid line shows the average n_σ at 333 K obtained using a ΔH of 2.92 kJ/mol per residue and a ΔC_p of 58 J mol^{-1} K^{-1} per residue (*83*). The two dotted lines show the average n_σ values at 318 and 348 K to provide the swath of T_m values for the proteins used in the plot. The dashed line at $n_\sigma = 3$ sets an approximate threshold between two-state-like and marginal barriers.

barrier of ~12RT at a midpoint temperature of 300 K). Incidentally, the 27% stabilization energy derived from this analysis is in very close agreement with the average ϕ value for these proteins (*56*). The striking similarity among six different proteins, which vary widely in size, structure, sequence, and thermodynamic parameters, immediately suggested a fundamental principle at work. It would be interesting to further explore this idea by extending the analysis to other slow two-state folding proteins.

This simple analysis provides a quantitative picture of the nature and heights of folding barriers that is consistent with physical theory. It is important, however, to develop methods for extracting folding barrier heights that do not require an empirical estimate for the diffusion coefficient. Barrier heights obtained with independent methods can be compared to test for consistency in the results. Moreover, once the barrier height has been measured with a different approach, eq 1 could be used backward to estimate effective diffusion coefficients from folding rates. Two independent methods that move in that direction have been recently developed.

The first procedure is based on scaling arguments from polymer physics. Scaling laws have been invoked to indicate that folding times should increase with N^υ, where N is the number of residues in the protein and υ an exponent smaller than 1 (*57*−*60*). This predicted scaling behavior became clearly apparent once a folding database with sufficient dynamic range in size was available (*61*). The correlation between rates and N gives a ruler for calculation of the average increase in barrier height per residue, but it does not provide the absolute magnitude of the barriers. The magnitude was estimated by noticing that the exponent of 1/2 proposed by Thirumalai (*57*) can be interpreted thermodynamically with the expression

$$n_\sigma = \Delta H(T)/\sqrt{RT^2\Delta C_p} \qquad (2)$$

where $\Delta H(T)$ is the equilibrium unfolding enthalpy at a given temperature and ΔC_p the change in heat capacity upon unfolding (*61*). n_σ represents the frequency at which the excess enthalpy fluctuations in the unfolded state reach enthalpy values characteristic of the native state. It is converted into free energy by calculating the height n_σ standard deviations from the minimum in a harmonic potential. These energies are temperature-dependent, but at 333 K, their values scale with N with exactly the same slope as the folding times (the ruler). The matching of slopes suggests that at 333 K solvation terms in ΔH and ΔC_p compensate exactly in eq 2 so that the calculated free energies approach the real barrier heights. The barriers obtained with this method are consistent with the estimates from eq 1. In fact, a plot of the barrier heights calculated from eq 2 at 333 K versus the logarithm of experimental folding rates (in energy units) crosses the zero barrier at ~1/(1 μs), providing an independent estimate of the average diffusion coefficient for folding (*61*). Another interesting aspect of this analysis is that it is entirely based on thermodynamic properties. Thermodynamic parameters obtained in equilibrium unfolding experiments are everything that is needed to catalog proteins according to their folding behavior. This is illustrated in Figure 3, which shows a plot of experimentally determined n_σ values versus N for a series of proteins with midpoint temperatures near 333 K. The $n_\sigma = 3$ line in the figure delimits the threshold separating two-state-like proteins from those that fold crossing marginal (or no) barriers. The figure reveals that individual proteins follow the general trend quite closely. Moreover, it indicates that proteins with fewer than 55 residues are expected to fold by crossing marginal barriers. For many of the proteins below the threshold in Figure 3, kinetic data showing folding on the microsecond time scale are available. It is also interesting that the de novo designed protein α3D (2A3D in Figure 3) is a clear outlier in the plot, featuring an n_σ smaller than that expected for its size. This observation suggests that the parameter n_σ could be used to gauge the compliance of designed proteins with their "natural" counterparts.

In the second method, thermodynamic barrier heights for folding are obtained from the analysis of DSC data (*62*). The fundamental idea here is to extract the probability density as a function of an order parameter by taking advantage of the known connection between the DSC thermogram of a protein and its folding partition function. Measuring the probability density is equivalent to mapping the complete one-dimensional free energy surface for folding (not just the difference between the minimum and the maximum). In a thermogram without additional sources of fluctuations (i.e., experimental noise, protein vibrational modes, and solvent−protein fluctuations), the probability density is obtained by calculating the inverse Laplace transform. When handling a real protein DSC thermogram, however, one must fit the experimental data to an idealized mathematical description

of the free energy surface. In this particular case, the free energy surface was represented by a Landau polynomial using enthalpy as the order parameter (*62*). The procedure is quite simple and involves fewer fitting parameters than even a chemical two-state fit. Of course, its great advantage is that it provides the folding free energy surface and with it the folding barrier height. Because it is an equilibrium method, it is ideally suited to the study of proteins with small barriers for which there is significant probability density at the saddle point. Indeed, the application of this procedure to many of the proteins for which $n_\sigma < 3$ in Figure 3 has confirmed that these proteins have marginal folding barriers or fold globally downhill (*63*). Perhaps more surprisingly, the method seems to effectively detect barriers of up to $\sim 8RT$ (20 kJ/mol), indicating that it can be used for many of the available two-state-like proteins. Furthermore, the thermodynamic barrier heights measured with this analysis strongly correlate with the experimental folding rates with a slope close to 1 (*63*). This important observation supports the validity of the free energy surface analysis of protein folding and suggests that folding energy landscapes of natural proteins are very smooth. The interesting question is then whether protein landscapes are fundamentally smooth (due to intrinsic properties of the interactions driving folding) or have been designed to be smooth by natural selection. This question can now be addressed experimentally by comparing the folding energy surfaces of natural versus de novo designed proteins (*64*).

Manifestations of Folding with Marginal (or No) Barriers

From the developments described in the previous sections, it is apparent that a significant number of proteins that have been, and will be, investigated are likely to have marginal folding barriers. Small proteins (i.e., fewer than 55 residues), particularly α-helical ones, are likely to have marginal folding barriers. All proteins that fold on the microsecond time scale are expected to fall directly into this category or even in the global downhill extreme case (see the next section). An important practical issue is how to distinguish between proteins that cross marginal barriers and those that can be reasonably well treated as two-state systems. This is important not only from the standpoint of reclassifying some of the proteins previously described as two-state but also in rationalizing observed deviations from two-state-like behavior. In the chemical paradigm, some of the deviations from two-state behavior are tackled by introducing an additional chemical state (i.e., an intermediate). A typical example is the interpretation of two observed kinetic phases as an indication of a kinetically populated intermediate. Other deviations are just ignored, or blamed on experimental uncertainties (*65*). In principle, the marginal barrier and two-state folding regimes could be simply distinguished by measuring the free energy barrier in a DSC experiment. However, it is also convenient to define an additional set of empirical criteria based on standard protein folding experiments. This set of criteria could be used as a checklist for experimentalists. Recent efforts along these lines have crystallized into a series of empirical criteria.

The dependence of the observed folding behavior on the specific experimental probe is possibly the best-known indicator of folding with marginal barriers (*66*). If folding barriers are very small or absent, perturbations in the free energy surface lead to large displacements in the position and depth of its minima. The properties of the ensemble should change in complex patterns, leading to potentially different observations with techniques that probe different structural features. The differences can be observed in both equilibrium and kinetic experiments (*66*). In its equilibrium version, this concept was exploited for the characterization of global downhill folding (*67*) (see the next section). The kinetic manifestations have been thoroughly investigated in recent experiments and simulations (*68*−*70*). The apparent lack of probe dependence is also frequently used as indication of two-state folding, but a negative criterion is always a much weaker criterion (*65*). A thorough application of nuclear magnetic resonance can eliminate this limitation altogether (see the next section), but it is also possible to exploit the spectroscopic properties of some of the commonly used low-resolution techniques. For α-helical proteins, for example, circular dichroism (CD) is particularly convenient. Exciton effects from the coupling of amide dipoles in the α-helix structure make its CD spectrum change linearly as the helix length increases (*71*). Therefore, the spectroscopic analysis of protein CD spectra can provide independent estimates of the α-helix content and average helix length. Figure 4 shows the results of such analysis for myoglobin (panel A) and the downhill-folding protein BBL (panel B). The CD spectra of myoglobin at different temperatures are consistent with a

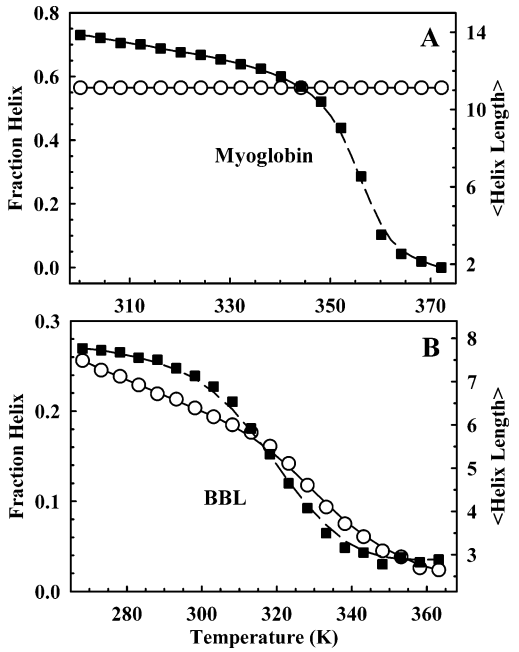

FIGURE 4: Analysis of far-UV CD spectra as a function of protein unfolding for the two-state protein myoglobin (A) and the global downhill protein BBL (B): average helical content (■, left scale) and average helix length (○, right scale). Experiments were performed in 20 mM phosphate buffer (pH 7.0). Each CD spectrum was fitted to the expression $\langle q(\lambda)\rangle = x_H[\theta_\lambda^\infty(1 - l_H/k_\lambda)] + (1 - x_H)\theta_\lambda^{coil}$, where x_H is the helix fraction, l_H is the average helix length, θ^∞ is the mean residue ellipticity of an infinite length helix as a function of wavelength (obtained from ref *71*), and k is the wavelength-dependent helix dependence of the CD spectrum (from ref *71*, and then further fitted to the lowest-temperature CD spectrum with the known x_H and l_H values from the structure). The latter was required to fine-tune structural details on each particular protein. θ^{coil} is the mean residue ellipticity as a function of wavelength of a random coil (taken as the CD spectrum of the protein under fully denaturing conditions).

helix signal constant in length (~11 residues) and a sigmoidal decrease in helix content, as expected for an all-or-none transition. For BBL, however, the helix content decays sigmoidally while the helix length decreases almost linearly across the whole temperature range. This observation is the basis for the CD wavelength dependence previously reported for BBL (*65*, *67*) and indicates that the three helices of BBL are unfolding in the complex manner expected for barrierless unfolding. A similar analysis in several other α-helical proteins suggests that this is a robust criterion for distinguishing between two-state and marginal (or no) barrier folding (unpublished data).

Another manifestation of folding with marginal barriers is the observation of significant unfolding occurring in the pre- and post-transition regions of the still sigmoidal unfolding curve. This behavior can be detected in a standard chemical two-state analysis by inspecting the physical properties of the native and unfolded phenomenological baselines. In a truly two-state system, the baselines should represent the properties of each of the two states as a function of the unfolding variable. If the folding reaction involves crossing a marginal (or no) barrier, these baselines embed some degree of unfolding and, thus, have values indicating structural changes as a function of the unfolding variable. The expected changes are highly sloped baselines that might even cross near the unfolding transition. This effect has been documented in CD baselines (*72*), but it is in the DSC experiment that it becomes very informative (*62*). The reason is that the DSC baselines directly report the energy fluctuations of the system, and the difference between the native and unfolded baselines renders the ΔC_p of unfolding. Furthermore, baseline effects on DSC experiments can be analyzed theoretically and have, indeed, been the subject of intense theoretical investigations by Chan and collaborators (*73*). Figure 5 shows DSC thermograms for free energy surfaces with a high barrier (~18 kJ/mol at the midpoint; see the inset), a marginal barrier (~3 kJ/mol at the midpoint; see the inset), and fully downhill. The three DSC thermograms can be fit well to a chemical two-state model (solid lines), as it has been discussed previously for experimental DSC data (*62*, *65*). However, comparison with the true theoretical DSC baseline reveals that the fitted native baseline becomes increasingly sloped and shifts to higher values (i.e., more disorder) as the barrier decreases. Furthermore, the native and unfolded baselines cross at increasingly lower temperatures. In fact, the baselines cross in the middle of the unfolding process for proteins with marginal barriers. This is unphysical because it implies that the ΔC_p changes sign in the middle of the transition. Thermograms with these features should be rigorously interpreted with the new methods for DSC analysis (see the previous section). However, even a simple two-state analysis of DSC data (measured in absolute heat capacity units so that baselines can be compared to pretabulated values) provides a first useful check.

The analysis of other classical equilibrium and kinetic experiments with the chemical two-state model provides additional criteria for marginal (or no) barrier folding. One such example is obtained from double perturbation equilibrium unfolding experiments. The coupling between two denaturing agents (e.g., temperature and chemical denaturant) is defined by straightforward Maxwell relationships for a

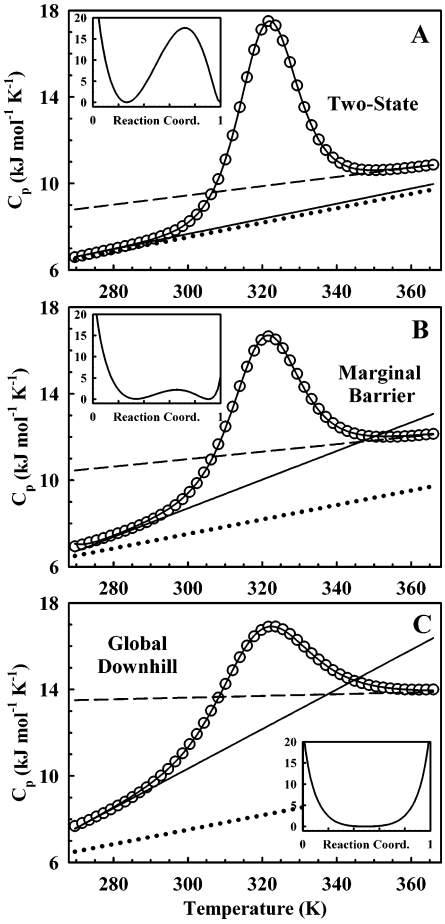

FIGURE 5: Simulated DSC thermograms for proteins with different folding barriers: (A) two-state-like (midpoint barrier of ~18 kJ/mol), (B) marginal barrier (midpoint barrier of ~2 kJ/mol), and (C) global downhill (no barrier at midpoint). The solid curves are two-state fits to the simulated data with solid and dashed lines representing the phenomenological baselines for the native and unfolded states, respectively. The dotted line shows the theoretical native heat capacity. Insets show the free energy barrier at the midpoint.

two-state system (*74*). For a protein with a marginal folding barrier, the coupling is more complex because the two agents change the properties of the ensemble in different ways (*72*). This phenomenon can be observed by simply plotting the change in unfolding enthalpy at a reference temperature (e.g., 298 K) as a function of the other denaturing agent (e.g., urea). The plot should be linear for a two-state system, while a protein with a marginal barrier or no barrier produces a curved profile (*65*). Another interesting criterion of two-state versus marginal (or no) barrier is provided by the sensitivity to chemical denaturants. A two-state protein should display the same sensitivity to chemical denaturants (i.e., *m* value) in equilibrium and kinetic experiments. By the same token, conservative single-point mutations of a two-state protein are expected to have *m* values similar to that of the wild type (*37*). It has been recently found that proteins with marginal (or no) free energy barriers are characterized by an underestimation of the equilibrium *m* value when measured kinetically. The underestimation is directly connected to the height of the barrier so that it becomes more severe as the barrier becomes smaller. The same effect is observed by comparing mutants of the same protein. Namely, the faster the relaxation rate of the mutant at its chemical midpoint,

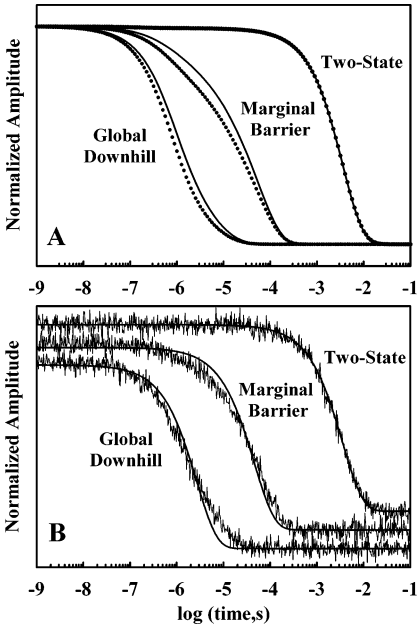

FIGURE 6: Folding kinetics at different barrier heights: (A) normalized relaxation kinetics in the folding direction (···) and unfolding direction (—) to the same final condition (near the midpoint) and (B) normalized relaxation kinetics with added noise and best fits to single-exponential decays.

the smaller the *m* value observed kinetically (A. N. Naganathan, U. Doshi, and V. Muñoz, unpublished results). This is a simple criterion that can be applied directly to data analyzed in the traditional chemical two-state fashion.

Finally, it is important to investigate some of the classical kinetic tests for two-state behavior. This can be done by simulating the kinetics of two-state, marginal barrier, and downhill folding as diffusion on the free energy surfaces shown in the insets of Figure 5. Figure 6 shows some of the results of such simulations at 324 K. The simulations show clearly that for a protein with a large barrier the relaxation rate is exponential and identical whether it is measured in the folding or unfolding direction. The global downhill protein folds much faster and with a relaxation that approximates a slightly stretched exponential. The marginal barrier protein displays a biexponential relaxation with two phases that differ by approximately 1 order of magnitude. For both marginal and global downhill folding, the apparent relaxation is faster when measured in the folding direction (panel A). The deviations from exponential kinetics are apparent even in noisy experimental kinetics traces (see panel B). For the marginal barrier case, deviations concentrate on the early times (missing the fast phase), while they are spread throughout the whole time course for global downhill folding. These results show that biexponential relaxations are a trademark of folding with marginal barriers. The two phases merge again into a more complex relaxation decay when the barrier disappears. The observation of biexponential kinetics has been documented in several fast-folding proteins (*35*, *75*−*80*). Gruebele and co-workers have interpreted this behavior as arising from a marginal barrier in the engineered λ repressor (*35*). However, a more common trend has been to discuss this observation in terms of a folding intermediate (i.e., a three-state system) (*75*, *76*, *78*−*80*). Given what we presently know about folding diffusion coefficients, the marginal barrier interpretation is much more likely to be correct for fast-folding proteins. Of course, this interpretation would be further strengthened if the protein complies with some of the other criteria for marginal barriers outlined above.

Global Downhill (One-State) Folding and Molecular Rheostats

The progress made in recent years in our understanding of folding barriers puts the experimental identification of global downhill, or one-state, folding (*67*) in the right perspective. Global downhill folding results from a free energy surface with only one well under all conditions. Under highly stabilizing conditions, the minimum of the well is located on the far right side of the reaction coordinate (i.e., native structure). As the native bias decreases, the minimum progressively shifts toward lower values of the reaction coordinate (i.e., more disorder). Under this one-state scenario, the unfolding transition is structurally continuous and the conformational ensemble populated under each condition corresponds to a different stage of the folding reaction (*67*). The experiments and analyses described above demonstrate that global downhill and two-state-like folding constitute the two extremes of a continuous folding scale in which barrier heights range from significantly high ($\sim$15*RT*) to nonexistent. Single-domain proteins that fold on the millisecond time scale or longer time scales are likely to behave in a two-state fashion. On the other hand, fast-folding small domains might fold crossing marginal barriers and, thus, display an apparently more complex folding behavior. The barrier might be negligible for some of the small fast-folding proteins, leading to the global downhill folding exhibited by BBL.

The discovery of one-state folding provides a unique opportunity to resolve folding mechanisms experimentally. The absence of a free energy barrier eliminates many of the technical limitations inherent to two-state folding. The three resolution requirements (structure, time, and statistics) can be split apart for global downhill folding because the properties of the ensemble are easily tuned. High-resolution NMR experiments can be used in equilibrium to characterize the average structural properties of the protein ensemble with atomic resolution. Under different stability conditions, the ensemble populates specific subgroups of conformations corresponding to the various stages of the reaction. The apparent unfolding curves of individual protein atoms can then show distinct behaviors depending on how their chemical shifts are perturbed by the varying structural features of the ensemble (*65*, *66*). If the degree of thermodynamic coupling between protein atoms is simply determined by their spatial proximity in the native structure, the distribution of atomic unfolding behaviors would be approximately Gaussian and span the global unfolding transition. Figure 7, in which the darker gray area defines the swath corresponding to behaviors within one standard deviation of the average unfolding curve (the circled line) and the lighter gray delimits the maximal spread expected for individual atoms, depicts this scenario. Measurement of 158 atomic unfolding curves for the BBL protein using NMR shows a distribution such as that of Figure 7 (*81*). In addition to providing a structural confirmation of global downhill folding, these observations can be exploited to measure folding cooperativity and map out the networks of interactions that stabilize protein structure (*81*). The NMR results

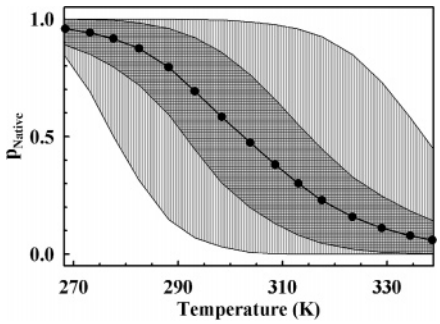

FIGURE 7: Equilibrium global downhill unfolding at atomic resolution. The circled line represents the average atomic unfolding behavior or global unfolding behavior (i.e., the behavior observed with a low-resolution technique). The dark gray swath corresponds to atomic unfolding behaviors within one standard deviation of the average. The light gray swaths represent the maximal spread of individual atomic unfolding behaviors, which should roughly correspond to the broadness of the global unfolding transition.

in BBL demonstrate that it is possible to resolve folding mechanisms in equilibrium experiments. Similarly, kinetic experiments of downhill folding could be used to directly measure folding diffusion coefficients as a function of the reaction coordinate. Global downhill folding is also well suited for analysis with single-molecule spectroscopic methods because it eliminates the need of resolving the sharp folding−unfolding transitions inherent to two-state folding.

The possible biological implications of one-state folding are also of interest. The classical view of protein function, in which proteins are switched from fully on to fully off by a discrete conformational change, is tightly connected to the two-state folding mechanism. In fact, it has been commonly assumed that proteins work as binary switches in a natural extension of their two-state (cooperative) folding behavior. However, from the analysis of folding free energy barriers, we now know that two-state folding is not an intrinsic property of proteins. Rather, it seems to be the product of careful selection by natural evolution, exactly as originally proposed by the energy landscape approach to protein folding (*3*). If evolutionary pressure is an important factor in achieving two-state folding, it is only natural to infer that the observation of one-state protein folding responds to the same evolutionary forces. The question is then what the biological role of one-state folding proteins could be. Their complex conformational behavior immediately suggests a role as molecular rheostats. We could think of one-state proteins working as instantaneous sensors, potentiometers, and oscillators. All of these functionalities could be engineered by coupling a signal to the continuous conformational changes characteristic of one-state folding. For example, an oscillator that synchronizes the action of three enzymes in a multistep reaction could be simply achieved by binding of the first and third enzymes to different conformational subensembles of a one-state (single-well) domain in the intermediate enzyme. The same oscillatory behavior can be exploited mechanically as a recoiling mechanism. Indeed, the molecular rheostat idea was put forward as an explanation for the complex functional roles that the small global downhill folder BBL plays in the oxo-glutarate dehydrogenase multienzyme complex (*67*). Other functionalities could be easily imagined: building a single-molecule instantaneous sensor simply requires coupling the binding of the molecule to be detected to the folding of a one-state domain so that increased ligand concentrations induce a continuous change in conformation (and thus a gradual response). To explore these possibilities in more depth, it is important to identify other one-state folding domains with potential to work biologically as rheostats. From a functional standpoint, small domains that perform multiple functions within large supramolecular assemblies are promising targets. From a folding standpoint, these small proteins will be more likely to fold in a one-state fashion if their structure is mostly α-helical and have very few aromatic residues in their hydrophobic core. Wang and collaborators have recently proposed a simple structural criterion (*82*), which could be used in combination with the other ideas outlined here in the pursuit of new examples of global downhill folding.

REFERENCES

1. Berne, B. J., Borkovec, M., and Straub, J. E. (1988) Classical and Modern Methods in Reaction-Rate Theory, *J. Phys. Chem. 92*, 3711−3725.
2. Hanggi, P., Talkner, P., and Borkovec, M. (1990) Reaction-rate theory: Fifty years after Kramers, *Rev. Mod. Phys. 62*, 251−341.
3. Bryngelson, J. D., Onuchic, J. N., Socci, N. D., and Wolynes, P. G. (1995) Funnels, Pathways, and the Energy Landscape of Protein Folding: A Synthesis, *Proteins: Struct., Funct., Genet. 21*, 167−195.
4. Onuchic, J. N., LutheySchulten, Z., and Wolynes, P. G. (1997) Theory of protein folding: The energy landscape perspective, *Annu. Rev. Phys. Chem. 48*, 545−600.
5. Daggett, V., and Levitt, M. (1993) Realistic Simulations of Native-Protein Dynamics in Solution and Beyond, *Annu. Rev. Biophys. Biomol. Struct. 22*, 353−380.
6. Berne, B. J., and Straub, J. E. (1997) Novel methods of sampling phase space in the simulation of biological systems, *Curr. Opin. Struct. Biol. 7*, 181−189.
7. Duan, Y., and Kollman, P. A. (1998) Pathways to a protein folding intermediate observed in a 1-microsecond simulation in aqueous solution, *Science 282*, 740−744.
8. Karplus, M., and McCammon, J. A. (2002) Molecular dynamics simulations of biomolecules, *Nat. Struct. Biol. 9*, 646−652.
9. Palmer, A. G. (1997) Probing molecular motion by NMR, *Curr. Opin. Struct. Biol. 7*, 732−737.
10. Jackson, S. E. (1998) How do small single-domain proteins fold? *Folding Des. 3*, R81−R91.
11. Tanford, C. (1968) Protein denaturation, *Adv. Protein Chem. 23*, 121−282.
12. Ikai, A., and Tanford, C. (1973) Kinetics of Unfolding and Refolding of Proteins. 1. Mathematical Analysis, *J. Mol. Biol. 73*, 145−163.
13. Baldwin, R. L. (1995) The Nature of Protein-Folding Pathways: The Classical Versus the New View, *J. Biomol. NMR 5*, 103−109.
14. Brooks, C. L. (1998) Simulations of protein folding and unfolding, *Curr. Opin. Struct. Biol. 8*, 222−226.
15. Snow, C. D., Nguyen, N., Pande, V. S., and Gruebele, M. (2002) Absolute comparison of simulated and experimental protein-folding dynamics, *Nature 420*, 102−106.
16. Garcia, A. E., and Onuchic, J. N. (2003) Folding a protein in a computer: An atomic description of the folding/unfolding of protein A, *Proc. Natl. Acad. Sci. U.S.A. 100*, 13898−13903.
17. Eaton, W. A., Muñoz, V., Thompson, P. A., Chan, C. K., and Hofrichter, J. (1997) Submillisecond kinetics of protein folding, *Curr. Opin. Struct. Biol. 7*, 10−14.
18. Gruebele, M. (1999) The fast protein folding problem, *Annu. Rev. Phys. Chem. 50*, 485−516.
19. Callender, R. H., Dyer, R. B., Gilmanshin, R., and Woodruff, W. H. (1998) Fast events in protein folding: The time evolution of primary processes, *Annu. Rev. Phys. Chem. 49*, 173−202.
20. Eaton, W. A., Muñoz, V., Hagen, S. J., Jas, G. S., Lapidus, L. J., Henry, E. R., and Hofrichter, J. (2000) Fast kinetics and mechanisms in protein folding, *Annu. Rev. Biophys. Biomol. Struct. 29*, 327−359.
21. Ferguson, N., and Fersht, A. R. (2003) Early events in protein folding, *Curr. Opin. Struct. Biol. 13*, 75−81.

22. Kubelka, J., Hofrichter, J., and Eaton, W. A. (2004) The protein folding 'speed limit', *Curr. Opin. Struct. Biol. 14*, 76−88.
23. Bryngelson, J. D., and Wolynes, P. G. (1989) Intermediates and Barrier Crossing in a Random Energy-Model (with Applications to Protein Folding), *J. Phys. Chem. 93*, 6902−6915.
24. Cho, S. S., Levy, Y., and Wolynes, P. G. (2006) P versus Q: Structural reaction coordinates capture protein folding on smooth landscapes, *Proc. Natl. Acad. Sci. U.S.A. 103*, 586−591.
25. Camacho, C. J., and Thirumalai, D. (1993) Kinetics and thermodynamics of folding in model proteins, *Proc. Natl. Acad. Sci. U.S.A. 90*, 6369−6372.
26. Boczko, E. M., and Brooks, C. L. (1995) First-Principles Calculation of the Folding Free-Energy of a 3-Helix Bundle Protein, *Science 269*, 393−396.
27. Zhou, Y. Q., and Karplus, M. (1997) Folding thermodynamics of a model three-helix-bundle protein, *Proc. Natl. Acad. Sci. U.S.A. 94*, 14429−14432.
28. Socci, N. D., Onuchic, J., and Wolynes, P. G. (1996) Diffusive dynamics of the reaction coordinate for protein folding funnels, *J. Chem. Phys. 104*, 5860−5868.
29. Muñoz, V., and Eaton, W. A. (1999) A simple model for calculating the kinetics of protein folding from three-dimensional structures, *Proc. Natl. Acad. Sci. U.S.A. 96*, 11311−11316.
30. Doshi, U., and Muñoz, V. (2004) Kinetics of α-helix formation as diffusion on a one-dimensional free energy surface, *Phys. Chem. 307*, 129−136.
31. Huang, C. Y., Getahun, Z., Wang, T., DeGrado, W. F., and Gai, F. (2001) Time-resolved infrared study of the helix-coil transition using ^{13}C-labeled helical peptides, *J. Am. Chem. Soc. 123*, 12111−12112.
32. Huang, C. Y., Klemke, J. W., Getahun, Z., DeGrado, W. F., and Gai, F. (2001) Temperature-dependent helix-coil transition of an alanine based peptide, *J. Am. Chem. Soc. 123*, 9235−9238.
33. Huang, C. Y., Getahun, Z., Zhu, Y. J., Klemke, J. W., DeGrado, W. F., and Gai, F. (2002) Helix formation via conformation diffusion search, *Proc. Natl. Acad. Sci. U.S.A. 99*, 2788−2793.
34. Doshi, U., and Muñoz, V. (2004) The principles of α-helix formation: Explaining complex kinetics with nucleation-elongation theory, *J. Phys. Chem. B 108*, 8497−8506.
35. Yang, W. Y., and Gruebele, M. (2003) Folding at the speed limit, *Nature 423*, 193−197.
36. Yang, W. Y., and Gruebele, M. (2004) Folding λ-repressor at its speed limit, *Biophys. J. 87*, 596−608.
37. Fersht, A. R., Matouschek, A., and Serrano, L. (1992) The Folding of an Enzyme. 1. Theory of Protein Engineering Analysis of Stability and Pathway of Protein Folding, *J. Mol. Biol. 224*, 771−782.
38. Oliveberg, M., Tan, Y. J., and Fersht, A. R. (1995) Negative Activation Enthalpies in the Kinetics of Protein Folding, *Proc. Natl. Acad. Sci. U.S.A. 92*, 8926−8929.
39. Muñoz, V., Thompson, P. A., Hofrichter, J., and Eaton, W. A. (1997) Folding dynamics and mechanism of β-hairpin formation, *Nature 390*, 196−199.
40. Thompson, P. A., Muñoz, V., Jas, G. S., Henry, E. R., Eaton, W. A., and Hofrichter, J. (2000) The helix-coil kinetics of a heteropeptide, *J. Phys. Chem. B 104*, 378−389.
41. Jones, C. M., Henry, E. R., Hu, Y., Chan, C. K., Luck, S. D., Bhuyan, A., Roder, H., Hofrichter, J., and Eaton, W. A. (1993) Fast Events in Protein Folding Initiated by Nanosecond Laser Photolysis, *Proc. Natl. Acad. Sci. U.S.A. 90*, 11860−11864.
42. Bieri, O., Wirz, J., Hellrung, B., Schutkowski, M., Drewello, M., and Kiefhaber, T. (1999) The speed limit for protein folding measured by triplet−triplet energy transfer, *Proc. Natl. Acad. Sci. U.S.A. 96*, 9597−9601.
43. Lapidus, L. J., Eaton, W. A., and Hofrichter, J. (2000) Measuring the rate of intramolecular contact formation in polypeptides, *Proc. Natl. Acad. Sci. U.S.A. 97*, 7220−7225.
44. Buscaglia, M., Schuler, B., Lapidus, L. J., Eaton, W. A., and Hofrichter, J. (2003) Kinetics of intramolecular contact formation in a denatured protein, *J. Mol. Biol. 332*, 9−12.
45. Krieger, F., Fierz, B., Bieri, O., Drewello, M., and Kiefhaber, T. (2003) Dynamics of unfolded polypeptide chains as model for the earliest steps in protein folding, *J. Mol. Biol. 332*, 265−274.
46. Sadqi, M., Lapidus, L. J., and Muñoz, V. (2003) How fast is protein hydrophobic collapse? *Proc. Natl. Acad. Sci. U.S.A. 100*, 12117−12122.
47. Pollack, L., Tate, M. W., Darnton, N. C., Knight, J. B., Gruner, S. M., Eaton, W. A., and Austin, R. H. (1999) Compactness of the denatured state of a fast-folding protein measured by submillisecond small-angle X-ray scattering, *Proc. Natl. Acad. Sci. U.S.A. 96*, 10115−10117.
48. Hagen, S. J., and Eaton, W. A. (2000) Two-state expansion and collapse of a polypeptide, *J. Mol. Biol. 301*, 1019−1027.
49. Akiyama, S., Takahashi, S., Kimura, T., Ishimori, K., Morishima, I., Nishikawa, Y., and Fujisawa, T. (2002) Conformational landscape of cytochrome *c* folding studied by microsecond-resolved small-angle X-ray scattering, *Proc. Natl. Acad. Sci. U.S.A. 99*, 1329−1334.
50. Qiu, L., Zachariah, C., and Hagen, S. J. (2003) Fast chain contraction during protein folding: "Foldability" and collapse dynamics, *Phys. Rev. Lett. 90*, 168103.
51. Hagen, S. J., Qiu, L. L., and Pabit, S. A. (2005) Diffusional limits to the speed of protein folding: Fact or friction? *J. Phys.: Condens. Matter 17*, S1503−S1514.
52. Hagen, S. J., Hofrichter, J., Szabo, A., and Eaton, W. A. (1996) Diffusion-limited contact formation in unfolded cytochrome *c*: Estimating the maximum rate of protein folding, *Proc. Natl. Acad. Sci. U.S.A. 93*, 11615−11617.
53. Kubelka, J., Chiu, T. K., Davies, D. R., Eaton, W. A., and Hofrichter, J. (2006) Sub-microsecond protein folding, *J. Mol. Biol. 359*, 546−553.
54. Akmal, A., and Muñoz, V. (2004) The nature of the free energy barrier to two-state folding, *Proteins: Struct., Funct., Bioinf. 57*, 142−152.
55. Luque, I., and Freire, E. (1998) Structure-based prediction of binding affinities and molecular design of peptide ligands, *Methods Enzymol. 295*, 100−127.
56. Sanchez, I. E., and Kiefhaber, T. (2003) Origin of unusual φ-values in protein folding: Evidence against specific nucleation sites, *J. Mol. Biol. 334*, 1077−1085.
57. Thirumalai, D. (1995) From minimal models to real proteins: Time scales for protein folding kinetics, *J. Phys. I 5*, 1457−1467.
58. Gutin, A. M., Abkevich, V. I., and Shakhnovich, E. I. (1996) Chain length scaling of protein folding time, *Phys. Rev. Lett. 77*, 5433−5436.
59. Wolynes, P. G. (1997) Folding funnels and energy landscapes of larger proteins within the capillarity approximation, *Proc. Natl. Acad. Sci. U.S.A. 94*, 6170−6175.
60. Finkelstein, A., and Badretdinov, A. Y. (1998) Rate of protein folding near the point of thermodynamic equilibrium between the coil and the most stable chain fold: Influence of chain knotting on the rate of folding, *Folding Des. 3*, 67−68.
61. Naganathan, A. N., and Muñoz, V. (2005) Scaling of folding times with protein size, *J. Am. Chem. Soc. 127*, 480−481.
62. Muñoz, V., and Sanchez-Ruiz, J. M. (2004) Exploring protein-folding ensembles: A variable-barrier model for the analysis of equilibrium unfolding experiments, *Proc. Natl. Acad. Sci. U.S.A. 101*, 17646−17651.
63. Naganathan, A. N., Sanchez-Ruiz, J. M., and Muñoz, V. (2005) Direct measurement of barrier heights in protein folding, *J. Am. Chem. Soc. 127*, 17970−17971.
64. Scalley-Kim, M., and Baker, D. (2004) Characterization of the folding energy landscapes of computer generated proteins suggests high folding free energy barriers and cooperativity may be consequences of natural selection, *J. Mol. Biol. 338*, 573−583.
65. Naganathan, A. N., Perez-Jimenez, R., Sanchez-Ruiz, J. M., and Muñoz, V. (2005) Robustness of downhill folding: Guidelines for the analysis of equilibrium folding experiments on small proteins, *Biochemistry 44*, 7435−7449.
66. Muñoz, V. (2002) Thermodynamics and kinetics of downhill protein folding investigated with a simple statistical mechanical model, *Int. J. Quantum Chem. 90*, 1522−1528.
67. Garcia-Mira, M. M., Sadqi, M., Fischer, N., Sanchez-Ruiz, J. M., and Muñoz, V. (2002) Experimental identification of downhill protein folding, *Science 298*, 2191−2195.
68. Yang, W. Y., and Gruebele, M. (2004) Detection-dependent kinetics as a probe of folding landscape microstructure, *J. Am. Chem. Soc. 126*, 7758−7759.
69. Ma, H. R., and Gruebele, M. (2005) Kinetics are probe-dependent during downhill folding of an engineered λ(6−85) protein, *Proc. Natl. Acad. Sci. U.S.A. 102*, 2283−2287.
70. Ma, H. R., and Gruebele, M. (2006) Low barrier kinetics: Dependence on observables and free energy surface, *J. Comput. Chem. 27*, 125−134.
71. Chen, Y.-H., Yang, J. T., and Chau, K. H. (1974) Determination of the helix and β form of proteins in aqueous solution by circular dichroism, *Biochemistry 13*, 3350−3359.

72. Oliva, F. Y., and Muñoz, V. (2004) A simple thermodynamic test to discriminate between two-state and downhill folding, *J. Am. Chem. Soc. 126*, 8596−8597.
73. Chan, H. S., Shimizu, S., and Kaya, H. (2004) Cooperativity principles in protein folding, *Methods Enzymol. 380*, 350−379.
74. Felitsky, D. J., and Record, M. T. (2003) Thermal and urea-induced unfolding of the marginally stable lac repressor DNA-binding domain: A model system for analysis of solute effects on protein processes, *Biochemistry 42*, 2202−2217.
75. Mayor, U., Johnson, C. M., Daggett, V., and Fersht, A. R. (2000) Protein folding and unfolding in microseconds to nanoseconds by experiment and simulation, *Proc. Natl. Acad. Sci. U.S.A. 97*, 13518−13522.
76. Mayor, U., Guydosh, N. R., Johnson, C. M., Grossmann, J. G., Sato, S., Jas, G. S., Freund, S. M., Alonso, D. O., Daggett, V., and Fersht, A. R. (2003) The complete folding pathway of a protein from nanoseconds to microseconds, *Nature 421*, 863−867.
77. Kubelka, J., Eaton, W. A., and Hofrichter, J. (2003) Experimental tests of villin subdomain folding simulations, *J. Mol. Biol. 329*, 625−630.
78. Vu, D. M., Myers, J. K., Oas, T. G., and Dyer, R. B. (2004) Probing the folding and unfolding dynamics of secondary and tertiary structures in a three-helix bundle protein, *Biochemistry 43*, 3582−3589.
79. Wang, T., Lau, W. L., DeGrado, W. F., and Gai, F. (2005) T-jump infrared study of the folding mechanism of coiled-coil GCN4-p1, *Biophys. J. 89*, 4180−4187.
80. Religa, T. L., Markson, J. S., Mayor, U., Freund, S. M. V., and Fersht, A. R. (2005) Solution structure of a protein denatured state and folding intermediate, *Nature 437*, 1053−1056.
81. Sadqi, M., Fushman, D., and Muñoz, V. (2006) Atom by atom analysis of global downhill protein folding, *Nature*, advance online publication June 14, 2006 (DOI 10.1038/Nature04589).
82. Zuo, G., Wang, J., and Wang, W. (2006) Folding with downhill behavior and low cooperativity of proteins, *Proteins: Struct., Funct., Bioinf. 63*, 165−173.
83. Robertson, A. D., and Murphy, K. P. (1997) Protein structure and the energetics of protein stability, *Chem. Rev. 97*, 1251−1267.

BI060643C